ECCOMAS Congress 2016
VII European Congress on Computational Methods in Applied Sciences and Engineering
M. Papadrakakis, V. Papadopoulos, G. Stefanou, V. Plevris (eds.)
Crete Island, Greece, 5–10 June 2016

DEFROSTER NOZZLE SHAPE OPTIMIZATION USING THE CONTINUOUS ADJOINT METHOD

L.A. Germanou[2,1], E.M. Papoutsis-Kiachagias[2], A. Delacroix[1] and K.C. Giannakoglou[2]

[1]Toyota Motor Europe NV/SA,
e-mail: antoine.delacroix@toyota-europe.com

[2] Parallel CFD & Optimization Unit, School of Mechanical Engineering, National Technical University of Athens, Greece,
e-mail: {lefkatza,vaggelisp}@gmail.com, kgianna@central.ntua.gr

Keywords: Continuous Adjoint Method, Shape Optimization, HVAC Defroster Nozzle, Defrosting–demisting performance.

Abstract. *This paper presents the use of the continuous adjoint method, developed by the Parallel CFD & Optimization Unit of National Technical University of Athens (NTUA) in the OpenFOAM environment, for the shape optimization of a passenger car defroster nozzle, including experimental validation performed at Toyota Motor Europe (TME). The defroster nozzle plays a major role in the demisting-defogging of the windshield, by blowing high velocity hot air jets supplied by the HVAC (Heating, Ventilation and Air Conditioning) unit of the vehicle. For a well–designed defroster nozzle, the time required for dispelling condensation or frost on the windshield must be reasonable; the nozzle must also have the capability to perform uniform defrosting from the bottom of the windshield to its top, without patches of condensation. In view of the above, an appropriate objective function, to be minimized, is the integral of the difference of the air velocity from a target (desirable) one over a thin control volume defined close to the windshield, inside the car cabin. To set up the optimization problem, the shape of a reference defroster nozzle is allowed to vary according to the morphing capabilities of a volumetric NURBS tool developed by NTUA; the latter is also used for deforming the computational mesh at each optimization cycle, by adapting it to the changed defroster shape. The CFD analysis is based on RANS, using the k-ϵ turbulence model. The optimization loop uses the gradient of the objective function with respect to the coordinates of the control points of a volumetric B–splines lattice, which is computed using the continuous adjoint method. Experimental tests performed to measure the actual velocity pattern on the windshield include velocity measurements with a hot-wire anemometer. A convincing comparison between CFD analysis and measurements is presented. The improved demisting performance of the geometry resulted from the adjoint optimization was also experimentally validated, using rapid prototyping to manufacture the designed defroster nozzle.*

1 INTRODUCTION

The safety and thermal comfort of automotive passengers are the most important factors in the development of the automotive HVAC system, [6]. HVAC is responsible for the demisting and defrosting of the vehicle's windows and for creating/maintaining a pleasant climate inside the cabin by controlling air humidity and temperature. The defroster nozzle, as part of the HVAC system of vehicles, plays a major role in the demisting-defrosting of the windscreen. Demisting refers to any function intended to remove a film of condensate from the internal face of the surface of the windscreen. Defrosting refers to any function intended to eliminate frost or ice from the external surface of the windscreen. The HVAC unit provides hot air to the nozzle which is, blowing high velocity air jets to the windscreen.

Among other, windshield defrosting performance constitutes a compulsory test according to national and international legislation since it has a significant impact on driving safety. The formation of frost on the windshield and front door glasses during cold season can be proved dangerous as it is veiling the drivers view and disturbing driving. Therefore, defroster performance is seriously taken into consideration during the design of HVAC system. On the other hand, the HVAC system has to meet the following performance requirements, [1]: (a) the time required for dispelling condensation or frost on the windshield must be reasonable and (b) uniform defrosting ideally on the whole surface of the windshield must be ensured, for the latter to become clear without being spotty or with condensation patches.

According to previous research [1, 4], the demist pattern is related to the air velocity distribution on the windshield, reflecting the defrosting performance to some extent. The defroster nozzle must, therefore, be designed to provide optimal air velocity distribution. This requirement is expressed in the form of an (integral) objective function to be minimized using a gradient–based optimization method.

CFD–based optimization methods based on either evolutionary algorithms or gradient–based optimization can be used for the design of the defroster nozzle. In the latter case, the adjoint method computes the gradient of the objective function with respect to (w.r.t.) the design variables, with a cost which is independent of the number of design variables. This paper presents the use of the continuous adjoint method, developed by NTUA [8, 9, 10, 11] and implemented within OpenFOAM, for the shape optimization of a passenger car defroster nozzle, including experimental validation performed at Toyota Motor Europe (TME).

To set–up the optimization problem, the shape of a reference defroster nozzle is morphed using a volumetric B–splines–based morphing tool; the same tool undertakes the deformation of the CFD mesh at each optimization cycle. The CFD analysis is based on RANS, using the k-ϵ turbulence model. The optimization loop uses the gradient of the objective function w.r.t. the coordinates of the volumetric B–splines lattice, computed using the adjoint method.

Experimental tests to measure the actual velocity pattern on the windshield including velocity measurements with a hot–wire anemometer, were performed at the TME premises, in Belgium. A convincing comparison between CFD analysis and measurements is presented at first. Then, the improved demisting performance of the nozzle geometry resulted from the adjoint optimization is confirmed on the basis of experiments; rapid prototyping techniques were used to manufacture the optimized nozzle.

2 CFD & EXPERIMENTAL ANALYSIS

The flow problem is governed by the RANS equations for steady-state, incompressible flow, coupled with a turbulence model. The mean flow equations are:

$$R^p = -\frac{\partial v_j}{\partial x_j} = 0 \tag{1}$$

$$R_i^v = v_j \frac{\partial v_i}{\partial x_j} - \frac{\partial}{\partial x_j}\Big[(\nu + \nu_t)\Big(\frac{\partial v_i}{\partial x_j} + \frac{\partial v_j}{\partial x_i}\Big)\Big] + \frac{\partial p}{\partial x_i} = 0 \qquad i = 1, 2, 3 \tag{2}$$

where v_i are the velocity components, p stands for static pressured divided by the constant density ρ, ν is the constant bulk viscosity and ν_t is the turbulent viscosity. Turbulent viscosity results from the solution of the k-ϵ model, [7], with wall functions near the solid walls.

The flow equations are solved in the computational domain shown in fig. 1. The blower of the HVAC unit provides the defroster nozzle with a high temperature airflow which, in turn, directs high velocity air jets towards the windshield. The air flows through the whole cabin of the car and exits through a flap located in the rear of the passenger compartment, to the outside. Thus, the inlet (S_I) to the domain corresponds to the inlet to the defroster nozzle, the outlet (S_O) is a rectangular patch located in the rear part of the cabin and solid walls (S_W) are the duct sidewalls and the internal surface of the cabin.

At S_I, Dirichlet boundary conditions are imposed on v_i, k and ϵ and a zero Neumann condition on p. At S_O, a zero Dirichlet condition is imposed on p together with zero Neumann ones on v_i, k and ϵ. No–slip boundary is imposed on the solid walls S_W, where k, ϵ are computed using wall functions and a zero Neumann condition is imposed on p.

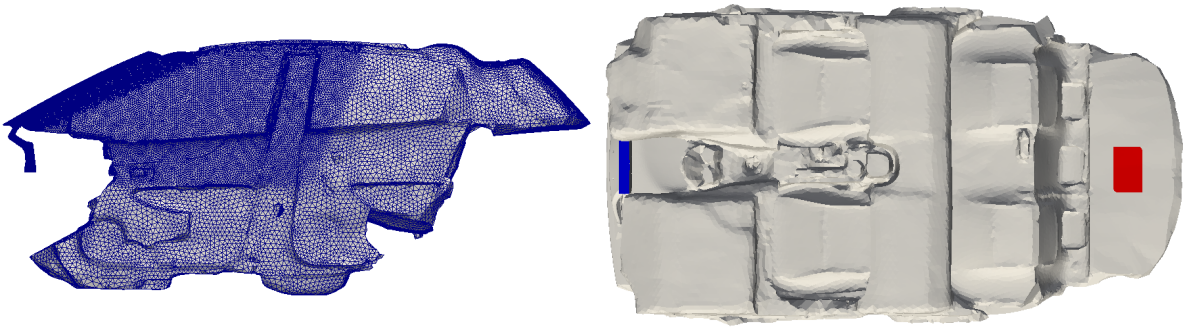

Figure 1: Side (left) and bottom (right) view of the computational domain Ω. On the left, the surface mesh is shown, highlighting the fact that the mesh is much finer inside the nozzle and in the front part of the cabin. S_I is in blue and corresponds to the inlet to the defroster nozzle. S_O, in red, is close to the trunk. The solid walls S_W correspond to the remaining surfaces of the cabin.

The flow equations are solved using the SIMPLE algorithm and a cell–centered finite–volume discretization scheme, on unstructured grids. The solution of the turbulence model PDEs is decoupled. Convection terms are discretized using a second-order upwind scheme, whereas for the computation of spatial gradients, the Green–Gauss theorem is used.

Before proceeding to the optimization, it is necessary to solve the flow problem, in the domain explained above, for the reference defroster nozzle. It should be noted that CAD data was only used for parts where high accuracy is necessary (defroster nozzle, windshield, instrument

panel close to the outlet of the nozzle, mirror). Already available laser scanned surface data was used for the remaining parts of the car cabin. Mesh refinement boxes were defined to achieve high accuracy where needed while balancing the overall computational cost, [5]. The mesh, provided by BETA CAE Systems to TME, is fine in the front cabin and coarser in the rear.

The Reynolds number of the flow is approximately 20000, based on the inlet hydraulic diameter. The flow fields over a cross section can be seen in fig. 2. The streamlines near the windshield can be seen in fig. 3.

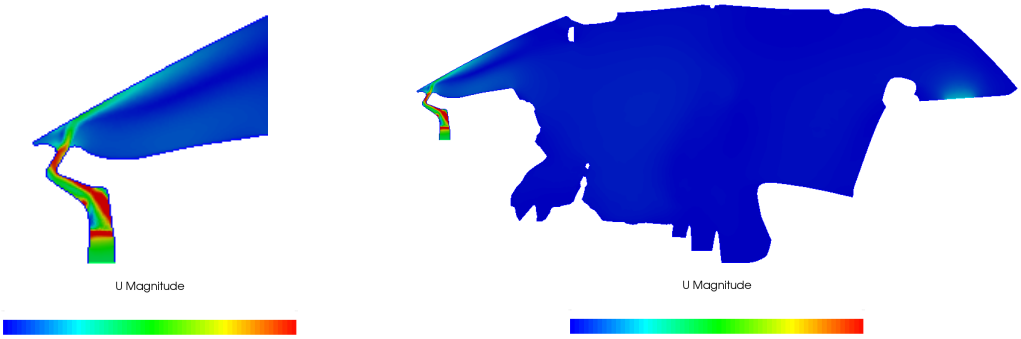

Figure 2: Velocity distribution across the symmetry plane; focus on the nozzle and windshield (left), the entire computational domain (right). The velocity magnitude is almost zero in the car cabin while, in the duct and close to the windshield, it reaches quite high values.

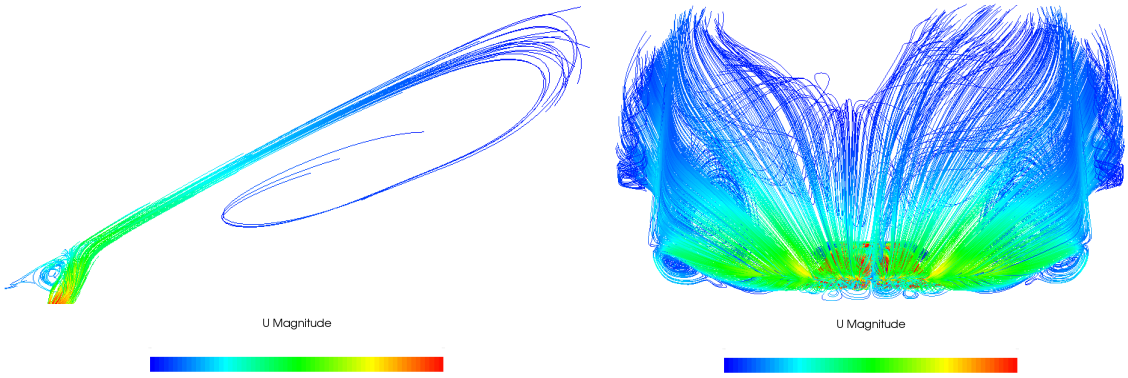

Figure 3: Streamlines emitted from seed points at the defroster inlet indicate the presence of small vortices of low velocity air at the bottom of the windshield, below the level where the jet flow starts to be attached to the windshield. The jet flow stays attached almost up to the level of the rear view mirror where recirculation occurs.

2.1 Experimental measurements–comparison

To verify the validity of the CFD results in the vicinity of the defroster nozzle jet flow and the internal surface of the windshield, [2, 3], a grid with 100mm spacing was drawn on the windshield, see fig. 4. The HVAC blower was controlled by constant voltage with an external power supply ensuring that the defroster nozzle provides constant airflow. Velocity was measured at each grid point using the hot–wire anemometer; all measurements were performed at points located on a surface 7mm away from the windshield, see also [2].

Figure 4: Set–up of the velocity pattern measurement. On the left, the 100mm–spaced grid is shown while, on the right, the use of the hot–wire anemometer on one of the grid points is demonstrated.

Measured and computed velocity patterns are compared in fig. 5. They are both non–symmetrical because the instrument panel is so. On the driver's side, the meter close to the steering wheel is creating this asymmetry that is affecting the flow exiting from the defroster nozzle, towards the windshield. Asymmetry is less intense on the CFD velocity pattern, since the HVAC blower was considered to provide uniform flow, which does not happen in reality. Regarding the measured velocity pattern, flow disturbance effects caused by the use of the measuring tool may have a small impact too. Moreover, during the measurement, the side defroster and face outlets were taped, so some leakage might be unavoidable. Last but not least, in a real car, air leakage occurs through the ducts and other parts, so the mass flow made available to the windshield through the defroster is lower than that provided from the blower, which was imposed as input to the CFD simulation.

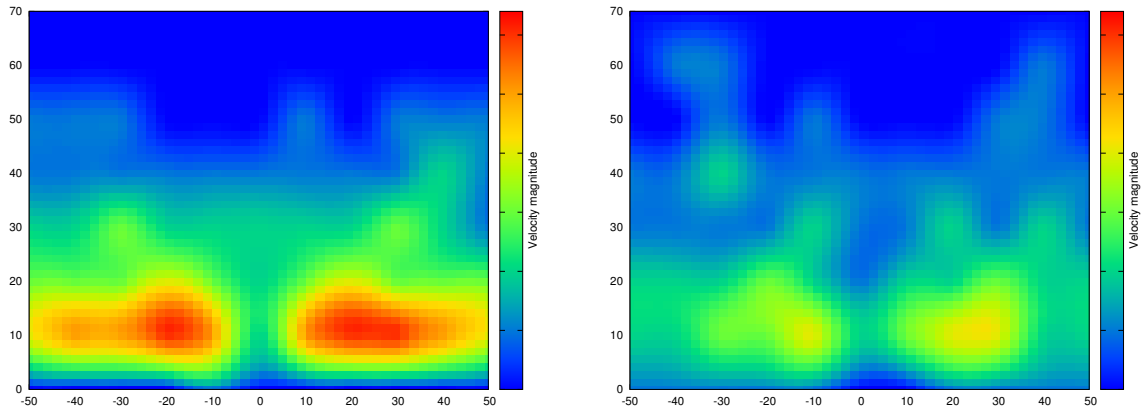

Figure 5: Comparison between CFD–predicted (left) and measured (right) velocity distributions close to the windshield. The axes are indicating the $2D$ grid used for the measurement (see fig. 4). CFD results and measurements have been similarly interpolated for better visualization. CFD analysis and measurements show similar trends.

The velocity pattern provided by the CFD run (post-processed on the basis of the computed velocity magnitude at the measurement points) gives a pattern qualitatively similar to the measured one. Quantitative differences between them can be due to the aforementioned reasons. Overall, the CFD simulation is considered to provide an acceptable flow prediction which allows to proceed to the adjoint–based optimization.

3 FORMULATION OF THE OPTIMIZATION PROBLEM–THE ADJOINT SOLVER

3.1 Objective function

It is desirable that the air velocity pattern close to the windshield meets some performance criteria pertinent to the improvement of the demisting and defrosting operation. Practically, a uniform velocity distribution close to the windshield is targeted. Given that the upper part of the windshield is dominated by low–velocity fluid flow, the objective function is confined to this upper half (hereafter, to be denoted by Ω_{tar}, figs. 6 and 7). There, target velocity v_{tar} should be higher than the flow velocity obtained with the reference defroster nozzle geometry. The objective function F is given by

$$F = \frac{1}{2}\int_{\Omega_{tar}} (v_i^2 - v_{tar}^2)^2 d\Omega \tag{3}$$

where Ω_{tar}, fig. 6 is referred to as the target volume.

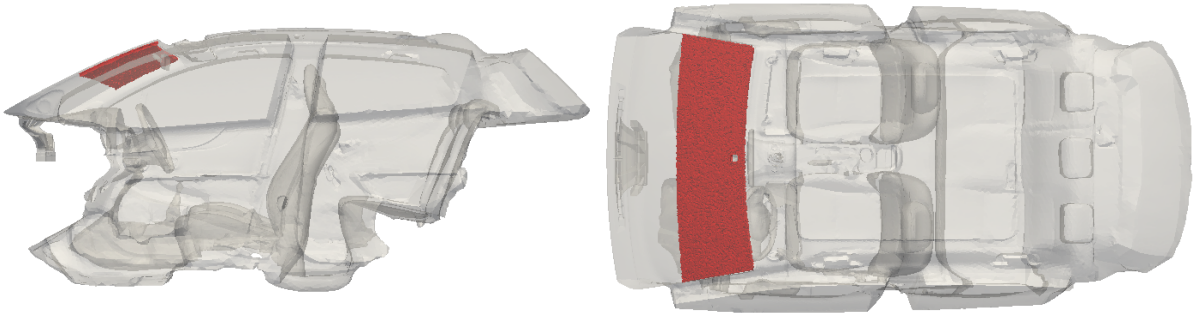

Figure 6: The thin target volume Ω_{tar} where the objective function is defined is marked in red, inside the computational domain Ω.

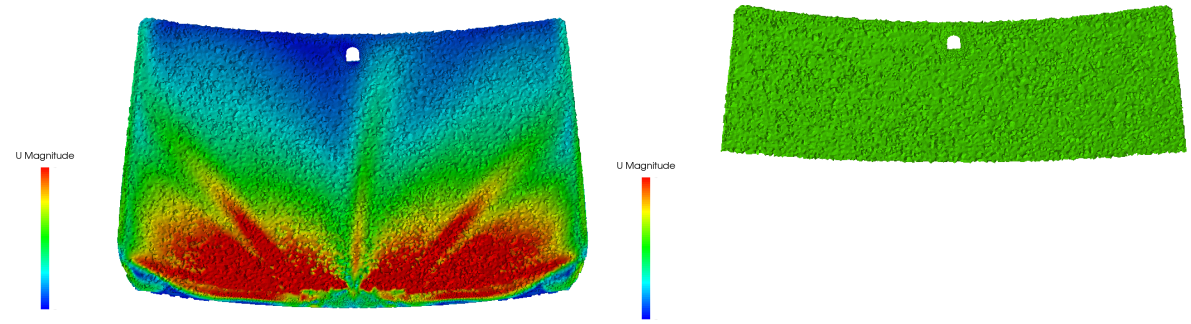

Figure 7: Velocity pattern computed by the CFD software (left). The velocity magnitude contours shown are 7mm away from the internal surface of the windshield. The air velocity distribution indicates low velocity areas in blue and high velocity areas in red. On the right, on the same color scale (indicating v_{tar}), the target volume (Ω_{tar}) is shown.

3.2 Optimization algorithm

To perform an automated CFD shape optimization loop for the defroster nozzle, the adjoint solver coupled with an in-house morpher was used, [11]. The shape morpher is based on volumetric B–splines [11], acting as a Free Form Deformation (FFD) method. The coordinates of the control points of the volumetric B–splines are the optimization variables b_n.

To start, the $3D$ morphing box enclosing the nozzle geometry to be optimized, the number of control points and the degree of the basis functions of the volumetric B–splines are defined. A structured control grid is generated. CFD mesh points residing within the control grid are identified and parameterized; by doing so, these can be displaced in conformity to the displacement of the control points during the optimization process. The flow and adjoint equations are solved and the objective function gradient w.r.t. b_n is computed. Having computed $\frac{\delta F}{\delta b_n}$, the control point coordinates are updated via steepest descent. The CFD mesh is also updated according to the nodal parametric coordinates which are assumed as constant during morphing. The previous steps are repeated until a termination criterion is met.

3.3 Adjoint equations & boundary conditions

The adjoint problem, which leads to the computation of the sensitivity derivatives consists of the adjoint mean flow equations

$$R^q = -\frac{\partial u_j}{\partial x_j} = 0 \tag{4}$$

$$R_i^u = u_j\frac{\partial v_j}{\partial x_i} - \frac{\partial (v_j u_i)}{\partial x_j} - \frac{\partial}{\partial x_j}\Big[(\nu+\nu_t)\Big(\frac{\partial u_i}{\partial x_j}+\frac{\partial u_j}{\partial x_i}\Big)\Big] + \frac{\partial q}{\partial x_i} + \underbrace{2(v_j^2 - v_{tar}^2)v_i}_{\textit{only in } \Omega_{tar}} = 0 \qquad i = 1,2,3 \tag{5}$$

where u_i is adjoint velocity and q is adjoint pressure as well as the adjoint boundary conditions, as explained in detail in [8, 9].

After satisfying the adjoint mean flow equations and their boundary conditions, the sensitivity derivatives are given by

$$\frac{\delta F}{\delta b_n} = -\int_{S_{W_P}} \Big[(\nu+\nu_t)\Big(\frac{\partial u_i}{\partial x_j}+\frac{\partial u_j}{\partial x_i}\Big)n_j - q n_i\Big]\frac{\partial v_i}{\partial x_k}\frac{\delta x_k}{\delta b_n}dS + \int_{S_{W_P}} (u_i R_i^v + q R^p)\frac{\delta x_k}{\delta b_n}dS \tag{6}$$

where, in the first term inside the brackets, there are only flow and adjoint variables while the outside part comes from the differentiation of the geometry, as computed by the morphing software. For the differentiation of the turbulence model, the reader should refer to [8, 9]

4 NUMERICAL OPTIMIZATION & VALIDATION

Before proceeding to the shape optimization of the defroster nozzle, the adjoint equations were solved in a domain associated with the reference geometry and the sensitivities of the objective function, eq. 6, w.r.t. the normal displacement of all surface mesh nodes were computed. These are shown in fig. 8, in the form of the so–called sensitivity map.

4.1 Optimization results

Several optimization runs were performed until the most suitable new shape of the defroster nozzle was obtained. The need to perform several optimization runs, instead of a single only, comes from the necessity of selecting the appropriate parameterization setup that gives more optimization potential, by also considering that the nozzle should be manufacturable and fit inside the assembly of its neighbouring parts. Manufacturing and topology constraints were manually taken into consideration during the optimization.

The designed (optimized) defroster nozzle yields 43% drop in the objective function and has the following characteristics as far as the parameterization set–up is concerned. Firstly, the

Figure 8: Sensitivity map indicating the change in the objective function F caused by the normal displacement of the boundary faces. Blue–colored areas should be pulled outwards while red areas should be pushed inwards so as to decrease the value of F.

control points were allowed to move only in the x–direction. Moreover, to get a quite smooth shape, the displacements per iso–plane were averaged, see fig. 10. In other words, all control points laying on the same iso–x plane are displaced in the x–direction using averaged sensitivity derivatives.

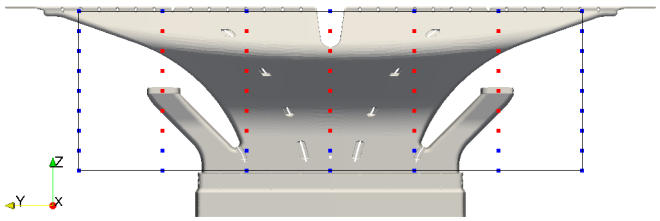

Figure 9: Control box ($3 \times 7 \times 9$) with active (red) and frozen (blue) control points. The frozen control points help to avoid mesh overlapping between the parameterized and non-parameterized areas. In this case, the side, top and two bottom rows of the control points are kept frozen.

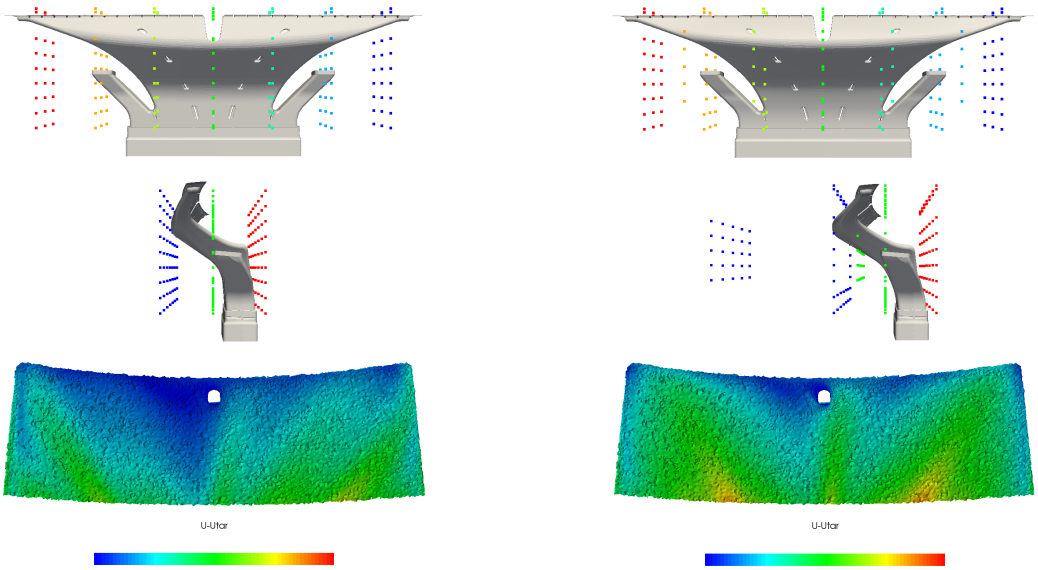

Figure 10: Reference (left) and optimized (right) defroster nozzle geometries and velocity patterns. In each row, the control grid nodes are colored based on a different coordinate. The final shape is very smooth, due to the averaging per iso–plane of the displacements of the control points and seems to be suitable for mass production. The field shown in the last row is $v - v_{tar}$ in which green areas correspond to areas where v_{tar} was reached, blue to areas with lower air velocity and red to areas with greater air velocity than the target. The comparison between the two patterns shows improvement in the coverage of the upper part of the windshield as well as increased uniformity. The target is practically reached over the majority of the cells of the target volume.

4.2 Defrost test of the optimized geometry & comparison

The optimized geometry of the defroster nozzle was manufactured using a rapid prototyping technique ($3D$ printing). Then, it was placed in the test vehicle, replacing the reference defroster nozzle and submitted to a defrost test. Windshield defrost patterns were obtained from cold room testing [3]. For the purpose of comparison, the defrosting and demisting efficiency of both the reference and optimized defroster nozzles have been tested.

To reproduce cold start condition, the vehicle soaked for several hours at a temperature of $-20°C$, in TME's climatic chamber. Following the soak, a high amount of humidity was generated in the cabin for a few minutes. Then, the defrost test commenced. The patterns were recorded regularly and the windshield was marked from the inside to indicate clearance areas.

The melting pattern for the reference and the improved defrosters, at two different time instants, are shown in fig. 11. At every instant recorded, the new defroster nozzle geometry gives a bigger clearance zone compared to the initial one. At the end, the new geometry is proved to be capable of clearing the windshield completely in 15% less time than the reference defroster nozzle.

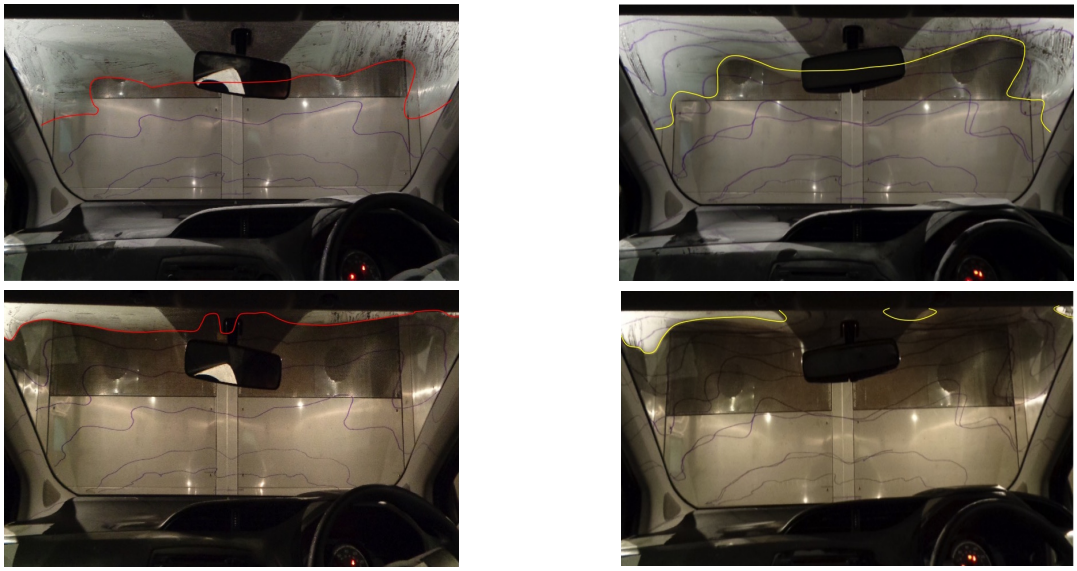

Figure 11: Defrost test of the reference (left) and improved (right) defroster nozzle shapes. The melting pattern is recorded and marked on the internal surface of the windshield. The patterns in the above figures are compared at the same time instants, proving the better defrosting ability of the optimized shape. The windshield with the optimized defroster nozzle shape is completely clear in 15% less time compared to the reference shape.

5 CONCLUSIONS

In this paper, shape optimization using the continuous adjoint method and a morphing software, both developed by the PCOpt Unit of NTUA, was applied to the defroster nozzle, part of the HVAC unit of a Toyota passenger car. A new defroster nozzle shape resulted, by maximizing the magnitude (according to a preset target value) and uniformity of the air velocity distribution on the upper–half of the windshield, leading improved defrosting performance of the vehicle. The optimized geometry, that was manually forced to comply with manufacturing and topological constraints, was manufactured with a rapid prototyping technique, placed in the vehicle and submitted to a defrost test that validated its improved defrosting performance. The optimized defroster nozzle achieves defrosting in 15% less time than the reference one.

ACKNOWLEDGMENTS

The contribution of BETA CAE Systems engineers in the pre–processing phase of the simulation is acknowledged.

REFERENCES

[1] T. Kohnotou, Y. Iwamoto, K. Hoshiawa, M. Nagataki, *Optimum Design of Defroster Nozzle.* SAE Technical Paper, 920167, 1992.

[2] B. S. AbdulNour, *Hot–Wire Velocity Measurements of Defroster and Windshield Flow.* Ford Motor Company, SAE Technical Paper, 970109, 1997.

[3] B. S. AbdulNour, *CFD Prediction of Automotive Windshield Defrost Pattern.* Ford Motor Company, SAE Technical Paper, 1999-01-1203, 1999.

[4] W. Yang, W. Shi, F. Guo, W. Yang, *Flow Field Simulation and Performance Analysis of HVAC Defrosting Duct.* 2nd International Conference on Electronic & Mechanical Engineering and Information Technology (EMEIT-2012), China, 2012.

[5] I. Goldasteh, S. Chang, S. Maaita, G. Mathur, *Numerical Simulation of Airflow Distribution on the Automobile Windshield in Defrost Mode.* SAE Technical Paper 2015-01-0330, doi:10.4271/2015-01-0330, 2015.

[6] J. Park and C. Kim, *Parametric Study on Automotive Windshield Defrost Pattern using CFD.* Hyundai MOBIS, SAE Technical Paper, 2003-01-1078, 2003.

[7] S.Patankar, D.Spalding, *Calculation Procedure for Heat, Mass and Momentum Transfer in Three–Dimensional Parabolic Flows.*, Int.J.Heat Mass Transfer Vol.15 pp.1787-1806, 1972.

[8] E.M. Papoutsis–Kiachagias, *Adjoint Methods for Turbulent Flows, Applied to Shape or Topology Optimization and Robust Design.* PhD Thesis, NTUA, 2013.

[9] E.M. Papoutsis–Kiachagias, K.C. Giannakoglou, *Continuous Adjoint Methods for Turbulent Flows, Applied to Shape and Topology Optimization: Industrial Applications.* Archives of Computational Methods in Engineering, DOI 10.1007/s11831-014-9141-9, 2014.

[10] E.M. Papoutsis–Kiachagias, A.S. Zymaris, I.S. Kavvadias, D.I. Papadimitriou, , K.C. Giannakoglou *The Continuous Adjoint Approach to the k–ϵ Turbulence Model for Shape Optimization and Optimal Active Control of Turbulent Flows.* Engineering Optimization, 47 (3), pp. 370-389, 2015.

[11] E.M. Papoutsis–Kiachagias, N. Magoulas, J. Mueller, C. Othmer, K.C. Giannakoglou, *Noise Reduction in Car Aerodynamics using a Surrogate Objective Function and the Continuous Adjoint Method with Wall Functions.* Computers and Fluids, 122, pp. 223-232, 2015.